

## 2D molybdenum and vanadium nitrides synthesized by ammoniation of 2D transition metal carbides (MXenes)

Patrick Urbankowski,<sup>1</sup> Babak Anasori,<sup>1</sup> Kanit Hantanasirisakul,<sup>1</sup> Long Yang,<sup>2</sup> Lihua Zhang,<sup>3</sup> Bernard Haines,<sup>1</sup> Steven J. May,<sup>1</sup> Simon J. L. Billinge,<sup>2,4</sup> Yury Gogotsi<sup>1†</sup>

<sup>1</sup>A.J. Drexel Nanomaterials Institute and Department of Materials Science & Engineering, Drexel University, Philadelphia, PA 19104, USA

<sup>2</sup>Department of Applied Physics and Applied Mathematics, Columbia University, New York, NY 10027, USA

<sup>3</sup>Center for Functional Nanomaterials, Brookhaven National Laboratory, Upton, NY 11973, USA

<sup>4</sup>Condensed Matter Physics and Materials Science Department, Brookhaven National Laboratory, Upton, NY 11973, USA

†Corresponding author:

Y. Gogotsi (gogotsi@drexel.edu) Tel.: +1-215-895-6446 Fax: +1-215-895-1934

### 1 Synthesis of Mo<sub>2</sub>Ga<sub>2</sub>C and Mo<sub>2</sub>CT<sub>x</sub>

*Synthesis of Mo<sub>2</sub>Ga<sub>2</sub>C:* Mo<sub>2</sub>CT<sub>x</sub> was synthesized by etching a Mo<sub>2</sub>Ga<sub>2</sub>C powder precursor. Mo<sub>2</sub>Ga<sub>2</sub>C powder was synthesized by a solid-liquid reaction in which -325 mesh Mo<sub>2</sub>C powder and Ga (both Alfa Aesar, Ward Hill, MA, 99.5 wt% purity) were mixed in a 1 : 8 molar ratio.<sup>1</sup> This mixture was placed in a quartz tube that was evacuated of air using a vacuum pump and then sealed.<sup>1</sup> The tube was then placed in a tube furnace that was heated to 850 °C at a rate of 10 °C min<sup>-1</sup>, and then held at that temperature for 48 h.<sup>1</sup> After the furnace cooled, the material was crushed using a mortar and pestle, and then returned to the quartz tube.<sup>1</sup> The tube was then evacuated and reheated to 850 °C at a rate of 10 °C min<sup>-1</sup> and then held for 16 h.<sup>1</sup> 1 g of Mo<sub>2</sub>Ga<sub>2</sub>C powder was washed in a 20 mL solution of 12 M hydrochloric acid (HCl) (technical grade, Fisher Scientific, Fair Lawn, NJ) for 48 h at room temperature (RT) while being stirred with a Teflon coated magnet on a stirring plate to remove any unreacted Ga.<sup>1</sup> The powders were washed with deionized (DI) water several times until a pH of 6 was reached, then filtered to dry the powder using a nanoporous polypropylene membrane (3501 Coated PP, 0.064 μm pore size, Celgard, USA).

*Synthesis of delaminated Mo<sub>2</sub>CT<sub>x</sub>:* 2 g of Mo<sub>2</sub>Ga<sub>2</sub>C powder was added to a bottle with 20 mL of 14 M HF solution (Fisher Scientific, Fair Lawn, NJ). Afterwards, the bottle was placed in an oil bath over a stirring hot plate and held at 55 °C for 72 h with stirring using a Teflon coated magnet in the bottle. The resulting suspension was washed with DI water several times until a pH of at least 6 was reached. Each time water was added to the centrifuge tube containing the product and water; it was then shaken before centrifuging at 3500 rpm for 2 min. The powder was then filtered and dried over a nanoporous polypropylene membrane (3501 Coated PP, 0.064 μm pore size, Celgard, USA). This product is referred to as multilayered Mo<sub>2</sub>CT<sub>x</sub>. 1 g of the powder was mixed with 10 mL of an aqueous solution of 54-56 wt.% tetrabutylammonium hydroxide (TBAOH) (Sigma Aldrich, St. Louis, MO, USA). The mixture was stirred for 1 h at RT. The mixture was then washed with 40 mL of DI water and centrifuged at 3500 rpm for 5 min. The mixture was washed three times. After washing, the powder sediment was bath

sonicated in a bottle of 50 mL of deionized water for 1 h. The suspension was then centrifuged at 3500 rpm for 1 h. The supernatant suspension was then filtered over nanoporous polypropylene membrane (3501 Coated PP, 0.064  $\mu\text{m}$  pore size, Celgard, USA). This yielded a film of delaminated  $\text{Mo}_2\text{CT}_x$  (d- $\text{Mo}_2\text{CT}_x$ ).

## 2 Synthesis of $\text{V}_2\text{C}$ and $\text{V}_2\text{CT}_x$

*Synthesis of  $\text{V}_2\text{AlC}$ :*  $\text{V}_2\text{CT}_x$  was synthesized by etching a  $\text{V}_2\text{AlC}$  powder precursor.  $\text{V}_2\text{AlC}$  powders were synthesized mixing -325 mesh vanadium, V and Al powders (both Alfa Aesar, Ward Hill, MA, 99.5 wt.% purity) and graphite, C (Alfa Aesar Ward Hill, USA, 99 wt.% purity; -300 mesh) were mixed in a 2.0 : 1.1 : 1.0 molar ratio.<sup>2</sup> The mixture was mixed and then placed in an alumina crucible boat which was placed in a tube furnace. The mixture was heated to 1600  $^\circ\text{C}$  at a rate of 5  $^\circ\text{C}/\text{min}$  under flow of argon, Ar, and held at that temperature for 4 h before cooling to RT. The resulting sintered blocks were milled using a titanium-nitride-coated milling bit to form powder. The powder was then sieved so that -400 mesh size particles were used for further treatment.

*Synthesis of delaminated  $\text{V}_2\text{CT}_x$ :* 2 g of  $\text{V}_2\text{AlC}$  powder was added to a bottle with 20 mL of 14 M HF solution (Fisher Scientific, Fair Lawn, NJ). Afterwards, the bottle was placed in an oil bath over a stirring hot plate and held at 35  $^\circ\text{C}$  for 24 h with stirring using a Teflon coated magnet in the bottle. The resulting suspension was washed with DI water several times until a pH of at least 6 was reached. Each time water was added to the centrifuge tube containing the product and water, it was then shaken before centrifuging at 3500 rpm for 2 min. The powder was then filtered and dried over a nanoporous polypropylene membrane (3501 Coated PP, 0.064  $\mu\text{m}$  pore size, Celgard, USA). This product is referred to as multilayered  $\text{V}_2\text{CT}_x$ . 1 g of the resulting powder was mixed with 10 mL of an aqueous solution of 54-56 wt.% tetrabutylammonium hydroxide (TBAOH) (Sigma Aldrich, St. Louis, MO, USA). The mixture was stirred for 1 h at RT. The mixture was then washed with 40 mL of DI water and centrifuged at 3500 rpm for 5 min. The mixture was washed three times. After washing, the powder sediment was bath sonicated in a bottle of 50 mL of deionized water for 1 h. The suspension was then centrifuged at 3500 rpm for 1 h. The supernatant suspension was then filtered over nanoporous polypropylene membrane (3501 Coated PP, 0.064  $\mu\text{m}$  pore size, Celgard, USA). This yielded a film of delaminated  $\text{V}_2\text{CT}_x$  (d- $\text{V}_2\text{CT}_x$ ).

*Ammoniation of delaminated MXene films:* Ammonia,  $\text{NH}_3$ , gas (anhydrous grade 4, Airgas, Philadelphia, PA, USA) flowing through a quartz tube in a Carbolite (Hope Valley, UK) tube furnace at a flowrate of 300  $\text{cm}^3/\text{min}$  was used to nitridize the MXene films. The samples were heated to 400  $^\circ\text{C}$ , 500  $^\circ\text{C}$  or 600  $^\circ\text{C}$  at a rate of 5  $^\circ\text{C}/\text{min}$  and dwelled at the target temperature for 1 h.

## 3 Scanning Electron Microscopy

To examine the morphology and composition of the nitrides, scanning electron microscopy (SEM) was performed in a Zeiss Supra 50VP (Carl Zeiss SMT AG, Oberkochen, Germany) equipped with an energy-dispersive X-ray spectrometer (EDX) (Oxford EDS, with INCA software). Most EDX scan were obtained at low magnification (100 $\times$  to 200 $\times$ ) on at least 3 different 0.5 mm  $\times$  0.5 mm areas for 60 s on each location. Atomic ratios determined from atomic percentages were calculated by averaging the atomic percentages of all points scanned. To determine if oxides were formed after ammoniation at 600  $^\circ\text{C}$ , micrographs of the  $\text{Mo}_2\text{N}$  and

V<sub>2</sub>N were taken, shown in Fig. S1. No separate cubic particles were found on the nitrides, confirming that no separate oxides were formed as a byproduct of this procedure or from oxidation of the nitride products.

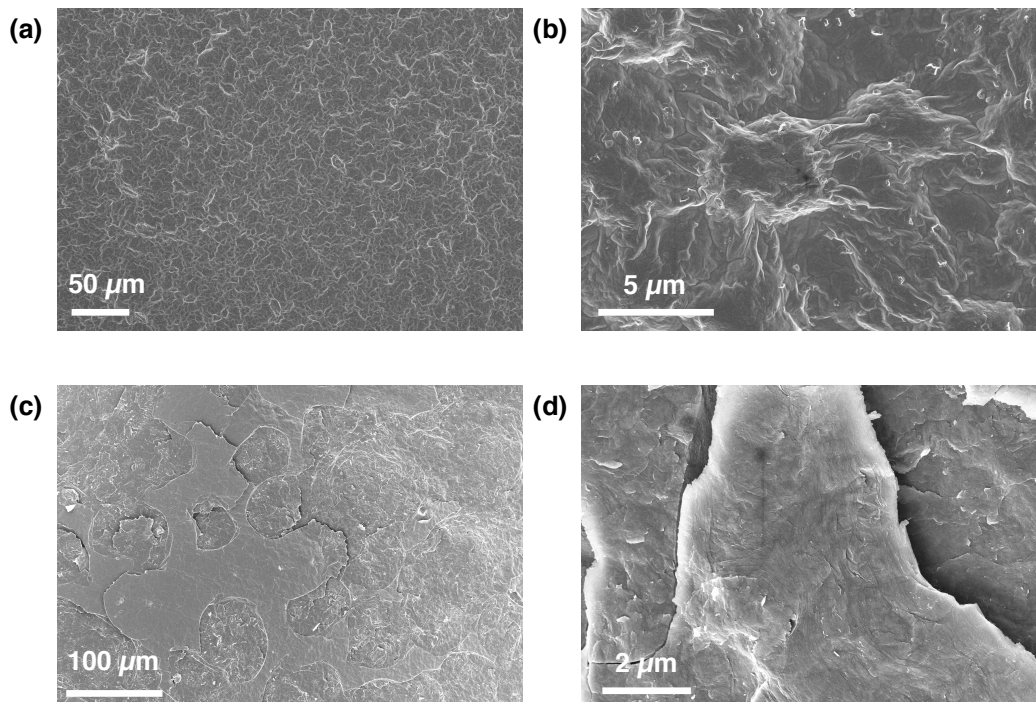


**Fig. S1.** Low and high magnification SEM images of Mo<sub>2</sub>N and V<sub>2</sub>N produced after annealing Mo<sub>2</sub>CT<sub>x</sub> and V<sub>2</sub>CT<sub>x</sub> films, respectively, in ammonia at 600 °C for 1 h. The absence of any cubic particles confirms that no oxides are formed from oxidation of the precursor MXene. (a) Low magnification of Mo<sub>2</sub>N. (b) High magnification image of Mo<sub>2</sub>N in (a). (c) Low magnification of V<sub>2</sub>N. (d) High magnification image of V<sub>2</sub>N in (c).

#### 4 X-ray Photoelectron Spectroscopy

X-ray photoelectron spectroscopy (XPS) spectra of the Mo<sub>2</sub>NT<sub>x</sub> and V<sub>2</sub>NT<sub>x</sub> films were measured by a spectrometer (Physical Electronics, VersaProbe 5000, Chanhassen, MN) employing a 100 μm monochromatic Al K $\alpha$  X-ray beam to irradiate each sample's surface. Photoelectrons were collected by a takeoff angle of 180° between the sample surface of each sample and the path to the analyzer. Charge neutralization was applied using a dual beam charge neutralizer irradiating low-energy electrons and ion beam to avoid shift in the recorded BE. High-resolution spectra for Mo 3d, C 1s, Mo 3p<sub>3/2</sub>, N 1s, V 2p and O 1s were taken at a pass energy of 11.75 eV with a step size of 0.05 eV. The binding energy scale of all XPS spectra was references to the Fermi-edge (E<sub>F</sub>), which was set to a BE of zero eV for each sample. The films were mounted on double-sided tape and were electrically grounded using a copper wire. Quantification and deconvolution of the core-level spectra was performed using a software package (CasaXPS Version 2.3.16 RP 1.6). Background contributions to the measured intensities were subtracted using a Shirley function prior to quantification and deconvolution. For the Mo<sub>2</sub>NT<sub>x</sub> film's spectra, intensity ratios of the 3d<sub>5/2</sub> and 3d<sub>3/2</sub> peaks were constrained to be 3:2. For the V<sub>2</sub>NT<sub>x</sub> film's spectra,

intensity ratios of the  $2p_{3/2}$  and  $2p_{1/2}$  peaks were constrained to be 2:1. The components of all regions scanned for for  $\text{Mo}_2\text{NT}_x$  are listed in Table S1. For  $\text{Mo}_2\text{N}$ , the high-resolution spectrum of the Mo 3d region (Figure S2a) were fitted by components corresponding to the two species N–Mo– $\text{T}_x$  and  $\text{MoO}_3$ . It is important to note that, for both the  $\text{Mo}_2\text{N}$  and  $\text{V}_2\text{N}$ , no F in XPS after the ammoniation of their MXene precursor, where F functional groups are typically detected.<sup>3</sup> The components of all regions scanned for for  $\text{V}_2\text{NT}_x$  are listed in Table S2. For  $\text{V}_2\text{NT}_x$ , the high-resolution spectrum of the V 2p region (Figure S2d) were fitted by components corresponding to the following four species: metallic V,  $\text{V}^{3+}$ ,  $\text{V}^{4+}$  and  $\text{V}^{5+}$ .

**Table S1.** Summary of global atomic compositions of the high resolution XPS region fittings of multilayered  $\text{Mo}_2\text{NT}_x$ , shown in Fig. 1c and Fig. S2a-c.

Region	BE [eV]	FWHM [eV]	Fraction	Assigned to	Reference
Mo $3d_{5/2}$ ( $3d_{3/2}$ )	229.0 (232.2)	1.0 (1.1)	0.21	N–Mo– $\text{T}_x$	4
	231.6 (235.3)	0.6 (1.1)	0.01	$\text{MoO}_3$	1
C 1s	283.1	0.9	0.01	C–Mo– $\text{T}_x$	4
	285.0	1.5	0.18	C–C	1
	286.6	1.4	0.03	$\text{CH}_x/\text{C–O}$	1
	288.7	2.0	0.02	COO	1
N 1s / Mo $3p_{3/2}$	395.1	2.5	0.21	Mo–N (Mo $3p_{3/2}$ )	4
	397.5	1.5	0.22	Mo–N (N 1s)	4
	399.2	2.0	0.02	$\text{MoO}_3$ (Mo $3p_{3/2}$ )	1
O 1s	530.9	1.4	0.03	N–Mo– $\text{O}_x$	1
	532.1	1.4	0.03	N–Mo–( $\text{OH}$ ) $_x$	1
	530.1	1.2	0.02	$\text{MoO}_3$	1
	533.6	1.5	0.01	N–Mo–OH– $\text{H}_2\text{O}$	1
Total			1.00		

**Table S2.** Summary of global atomic compositions of the high resolution XPS region fittings of multilayered  $\text{V}_2\text{NT}_x$ , shown in Fig. 1d and Fig. S2d-f.

Region	BE [eV]	FWHM [eV]	Fraction	Assigned to	Reference
C 1s	284.8	1.6	0.18	C–C	5
	286.3	1.4	0.04	$\text{CH}_x/\text{C–O}$	5
	288.0	2.0	0.03	C–N	5
N 1s	396.9	1.2	0.18	V–N	6
	398.3	3.2	0.11	N–C	7
V $2p_{3/2}$ ( $2p_{1/2}$ )	513.2 (520.2)	0.6 (1.2)	0.02	$\text{V}^{0+}$	8
	514.1 (521.3)	1.8 (2.2)	0.21	$\text{V}^{3+}$ (V–N)	9
	516.0 (523.0)	1.5 (1.5)	0.09	$\text{V}^{4+}$	8
	517.1 (524.6)	1.5 (1.8)	0.04	$\text{V}^{5+}$	8
O 1s	530.1	1.7	0.07	V–O	8
	532.0	2.0	0.03	N–O	10
Total			1.00		



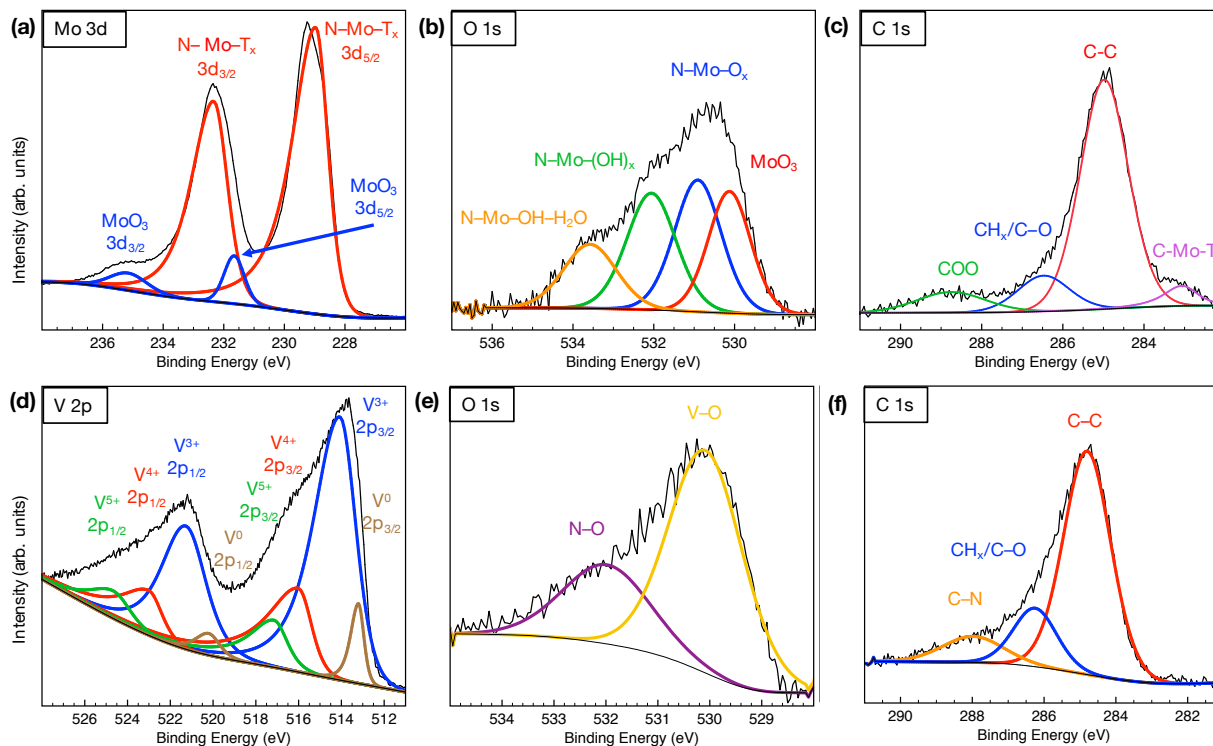


**Figure S2.** (a-c) High resolution XPS spectra for  $\text{Mo}_2\text{NT}_x$  synthesized by annealing delaminated  $\text{Mo}_2\text{CT}_x$  at 600 °C for 1 h in  $\text{NH}_3$  (ammonia). Regions for  $\text{Mo}_2\text{NT}_x$  shown are (a) Mo 3d, (b) O 1s and (c) C 1s, showing evidence of Mo–N bonding in (a). (d-f) High resolution XPS spectra for  $\text{V}_2\text{NT}_x$  synthesized by annealing delaminated  $\text{V}_2\text{CT}_x$  at 600 °C for 1 h in ammonia. Regions scanned for  $\text{V}_2\text{NT}_x$  shown are (d) V 2p, (e) O 1s and (f) C 1s.

## 5 X-ray Diffraction

X-ray diffraction (XRD) was carried out on the  $\text{Mo}_2\text{CT}_x$ ,  $\text{V}_2\text{CT}_x$ ,  $\text{Mo}_2\text{NT}_x$  and  $\text{V}_2\text{NT}_x$  films using a Rigaku Smartlab (Tokyo, Japan) diffractometer with  $\text{Cu-K}\alpha$  radiation (40 kV and 44 mA); step size 0.02°, 3-50°  $2\theta$  range, step time of 1 s,  $5 \times 10 \text{ mm}^2$  window slit. To investigate the change in crystal structure as temperature of ammoniation increases, XRD was performed after ammoniation of the  $\text{Mo}_2\text{CT}_x$  and  $\text{V}_2\text{CT}_x$  at 400 °C or 500 °C for 1 h, shown in Fig. S3. For  $\text{Mo}_2\text{NT}_x$ , the basal plane (002) MXene peak increases from  $2\theta = 7^\circ$  to  $9^\circ$ , indicating that the layered sheets are being annealed and more closely spaced. A peak at  $25^\circ$ , the source of which is uncertain, becomes more prominent but vanishes if the  $\text{Mo}_2\text{CT}_x$  is annealed at 600 °C instead of the temperatures below 600 °C. For the  $\text{V}_2\text{NT}_x$  patterns, the broad peak at  $2\theta = 25^\circ$  can be attributed to the glass slide on which the films were scanned.<sup>11</sup> A peak at  $37^\circ$  becomes more and more prominent as ammoniation temperature increases, which may possibly be a competing non-MXene nitride phase.

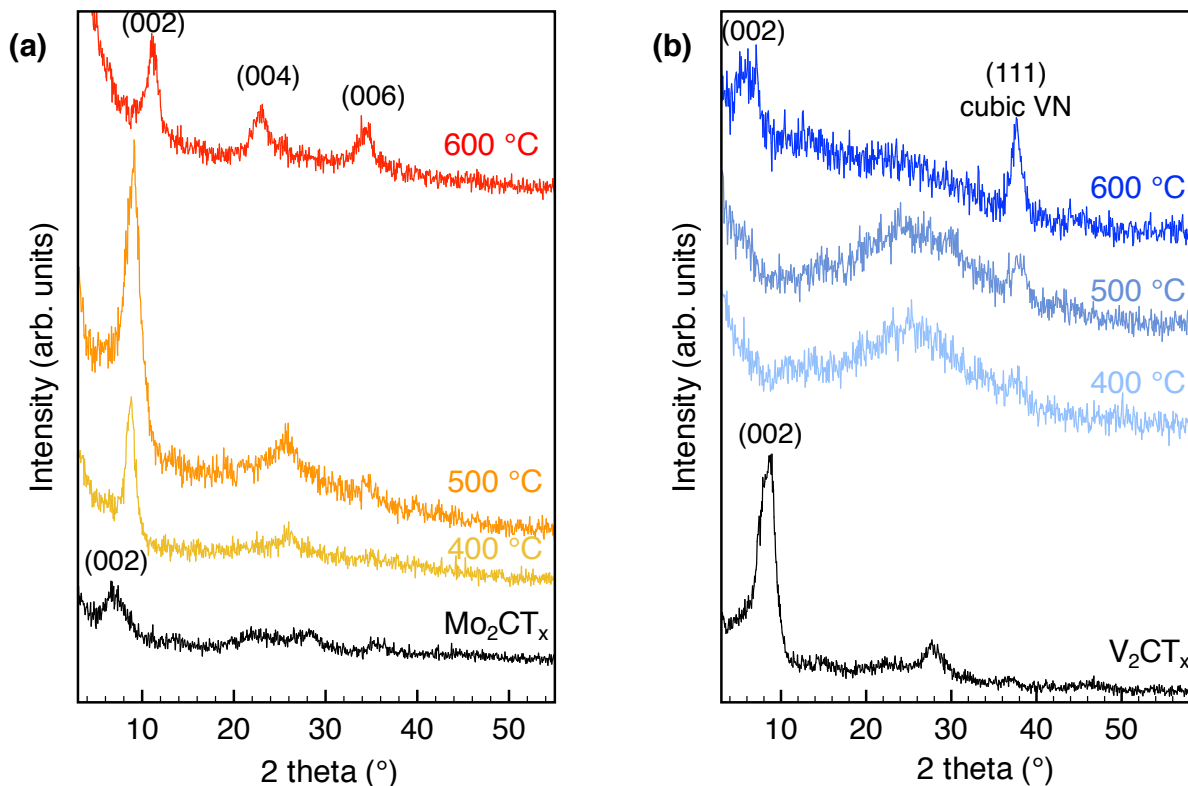


**Figure S3.** XRD patterns of (a)  $\text{Mo}_2\text{CT}_x$  and (b)  $\text{V}_2\text{CT}_x$  before and after ( $\text{Mo}_2\text{NT}_x$  and  $\text{V}_2\text{NT}_x$ ) ammoniation in ammonia gas at various temperatures for 1 h. (a) For  $\text{Mo}_2\text{NT}_x$ , as the temperature of ammoniation increases, the (002) peak shifts from  $\sim 7^\circ$  to  $\sim 11^\circ$  at  $600^\circ\text{C}$ . At ammoniation temperatures below  $600^\circ\text{C}$ , a peak at about  $25^\circ$  becomes more prominent, but vanishes when nitridation temperature increases to  $600^\circ\text{C}$ . (b) For  $\text{V}_2\text{NT}_x$ , as temperature of ammoniation increases, the peak at  $37^\circ$ , corresponding to a cubic VN, becomes more prominent.

## 6 X-ray Pair Distribution Function (PDF) Analysis

Synchrotron X-ray total scattering experiments were carried out at the X-ray Powder Diffraction (XPD) beamline, 28-ID-2, at the National Synchrotron Light Source II (NSLS II) at Brookhaven National Laboratory (BNL). The samples were crushed into powders, packed into 1 mm inner diameter kapton capillary tubes and measured at 100 K using a flowing nitrogen cryocooler. The rapid acquisition PDF technique (RaPDF)<sup>12</sup> was used with an X-ray energy of 67.14 keV ( $\lambda = 0.1847 \text{ \AA}$ ). A large area 2D Perkin Elmer detector ( $2048 \times 2048$  pixels and  $200 \times 200 \mu\text{m}$  pixel size) was mounted orthogonal to the beam path with sample-to-detector distance of 205.39 mm behind the samples. The raw 2D data were azimuthally integrated and converted to 1D intensity versus the magnitude of the scattering momentum transfer  $Q$  using FIT2D.<sup>13</sup>  $Q = 4\pi \sin \theta / \lambda$  for a scattering angle of  $2\theta$  and an X-ray wavelength of  $\lambda$ . The software xPDFsuite<sup>14, 15</sup> was used to correct and normalize the diffraction data and then Fourier transform them to obtain the experimental PDF,  $G(r)$ , according to:

$$G(r) = \frac{2}{\pi} \int_{Q_{\min}}^{Q_{\max}} Q[S(Q) - 1] \sin(Qr) dQ$$

where the total scattering structure function  $S(Q)$  is the properly corrected and normalized powder diffraction intensity measured from  $Q_{min}$  to  $Q_{max}$ , governed by the experimental setup.<sup>16</sup>  $G(r)$  gives the probability of finding a pair of atoms separated by a distance of  $r$ . Nickel was measured as the standard material to calibrate the sample-to-detector distance and to determine the  $Q_{damp}$  and  $Q_{broad}$  which are parameters that correct the PDF envelope function for the instrument resolution effects.<sup>17, 18</sup> The refined values  $Q_{damp} = 0.0369 \text{ \AA}^{-1}$  and  $Q_{broad} = 0.0131 \text{ \AA}^{-1}$  were fixed in the subsequent structure refinements of the PDF data. Structural modeling and refinement of PDF data was carried out using the PDFgui<sup>18</sup> and DiffPy-CMI programs.<sup>19</sup> Least-squares fits were performed by minimizing the fit residual, with the goodness-of-fit  $R_\omega$ , given by:

$$R_\omega = \sqrt{\frac{\sum_{i=1}^n [G_{obs}(r_i) - G_{calc}(r_i, P)]^2}{\sum_{i=1}^n G_{obs}(r_i)^2}}$$

where  $G_{obs}$  and  $G_{calc}$  are the experimental and calculated PDFs and  $P$  is the set of parameters refined in the model.

### 6.1 Structure Refinement of $V_2N$

The initial structural model for the  $V_2N$  was a trigonal  $P\bar{3}1m$  structure and the atoms are on the following special positions: V ( $x, 0, z$ ), N1 ( $1/3, 2/3, 1/2$ ), and N2 ( $0, 0, 0$ ) shown in Fig. S4.<sup>20</sup> The structure refinements were performed over full- $r$  (1.5 to 60  $\text{\AA}$ ), low- $r$  (1.5 to 20  $\text{\AA}$ ), and high- $r$  (20 to 60  $\text{\AA}$ ) ranges separately, as shown in Fig. S5.

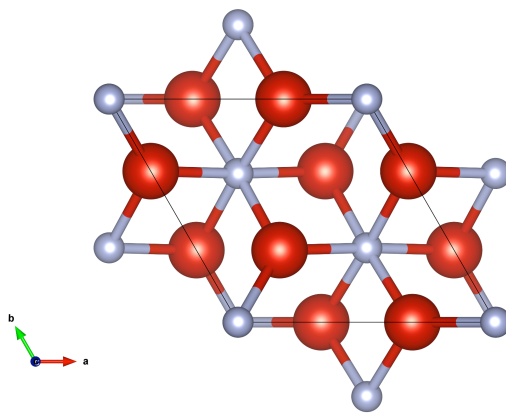


**Figure S4.** Trigonal  $V_2N$  (space group  $P\bar{3}1m$ ) structure projected along the  $[001]$  direction. Red atoms indicate V, blue atoms indicate N.

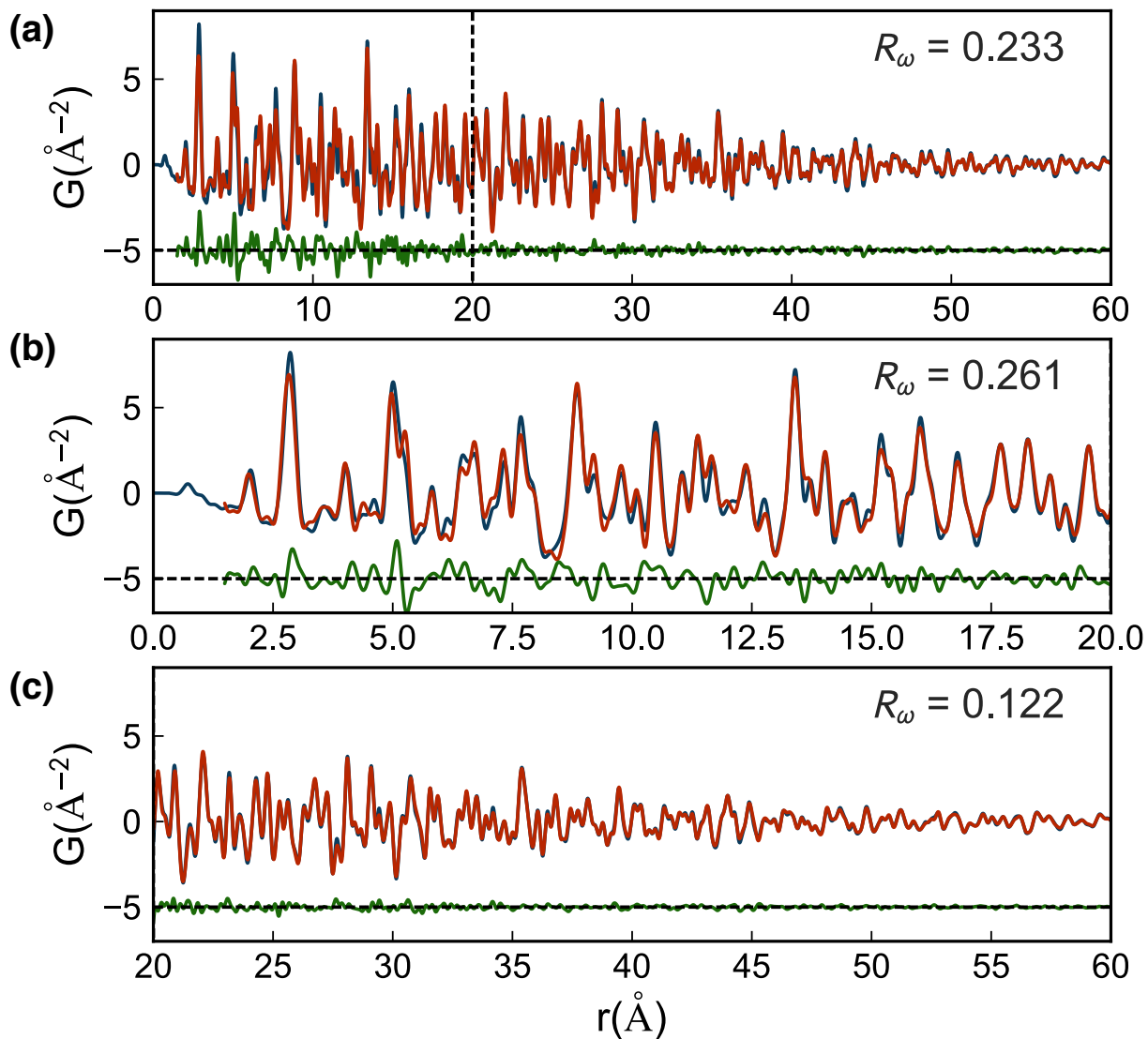


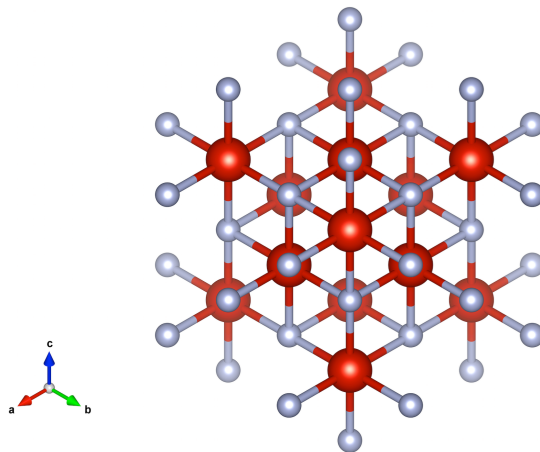
**Figure S5.** PDF fits (red curve) of the  $V_2N$  structure model to the measured data (blue) with difference curve offset below (green) over (a) full- $r$  (1.5 to 60 Å), (b) low- $r$  (1.5 to 20 Å), and (c) high- $r$  (20 to 60 Å) ranges.

**Table S3.** Structure refinement results of V<sub>2</sub>N structure model in the *r*-range of 1.5 to 60 Å, 1.5 to 20 Å, and 20 to 60 Å.

Fitting Range (Å)	1.5 to 60	1.5 to 20	20 to 60
$R_\omega$	0.233	0.261	0.122
$a$ (Å)	5.0421	5.0415	5.0423
$c$ (Å)	4.3712	4.3717	4.3714
$x$ (V)	0.6670	0.6671	0.6705
$z$ (V)	0.7452	0.7449	0.7500
$U_{iso}(V)$ (Å <sup>2</sup> )	0.0037	0.0033	0.0034
$U_{iso}(N)$ (Å <sup>2</sup> )	0.0326	0.0242	0.0144

$R_\omega$  of the high-*r* region (20 to 60 Å) fit, 0.122, is much lower than that of low-*r* region (1.5 to 20 Å), 0.261. This indicates that the V<sub>2</sub>N (space group  $P-31m$ ) structural model fits the long-range (20 to 60 Å) features well, but it does not describe the local structure completely. Because of this, a two-phase fit over the low-*r* range (1.5 to 20 Å) was then attempted.

To improve the local structure refinement, another phase, VN (space group is  $Fm-3m$ ), shown in Fig. S6, was added as a second phase with a finite particle size. The atoms are on the following positions: V at (0, 0, 0) and N at (1/2, 1/2, 1/2).<sup>21</sup>

**Figure S6.** Cubic VN (space group  $Fm-3m$ ) structure projected along the [111] direction. Red atoms indicate V, blue atoms indicate N.

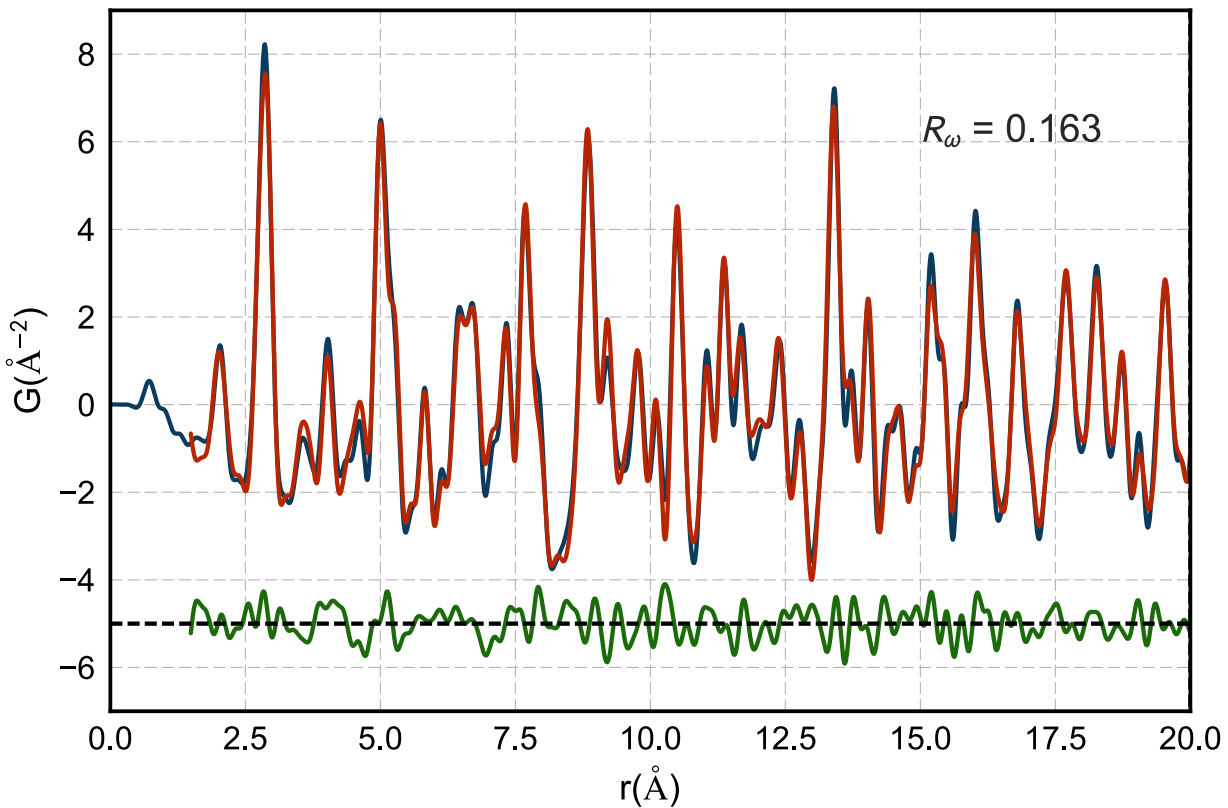


**Figure S7.** PDF fit (red curve) of the  $V_2N+VN$  mixed phase model to the measured data (blue) with difference curve offset below (green).

**Table S4.** Structure refinement result of  $V_2N + VN$  structure model in the  $r$ -range of 1.5 to 20 Å. For the VN phase, its lattice parameters were constrained as  $a = c$  due to cubic symmetry, and its isotropic atomic displacement parameters  $U_{iso}(V)$  and  $U_{iso}(N)$  were constrained the same as those in the  $V_2N$  phase. Spdiameter is the particle diameter parameter for PDF shape damping function.

Fitting Range (Å)	1.5 to 20 Å	
$R_\omega$	0.163	
Phase	$V_2N$	VN
Mass Ratio	68%	32%
$a$ (Å)	5.0382	4.1328
$c$ (Å)	4.3748	4.1328
$x$ (V)	0.6680	-
$z$ (V)	0.7511	-
$U_{iso}(V)$ (Å <sup>2</sup> )	0.0033	0.0033
$U_{iso}(N)$ (Å <sup>2</sup> )	0.0110	0.0110
Spdiameter (Å)	-	22.3461

Comparing with the structure refinement result of  $V_2N$  in Table S2, the two-phase fit over the low- $r$  range, 1.5 to 20 Å, ( $R_\omega = 0.163$ ) describes the local structure much better than the single-phase  $V_2N$  fit over the low- $r$  range ( $R_\omega = 0.261$ ). The PDF fit of this mixed phase model over the full- $r$  range (1.5 to 60 Å) is shown in Fig. 2b in the main text. The structure of Vanadium compound can be described as trigonal  $V_2N$  along with nanosized cubic VN.

## 6.2 Structure Refinement of $Mo_2N$

The  $Mo_2N$  single slab model (Fig. 2c in the main text) was initially built from the precursor  $Mo_2C$  MXene ( $P6_3/mmc$ ) structure by replacing N atoms with C atoms at the same atomic positions, then cutting a single slab of atoms from its respective bulk crystal structure. The atoms are on the following special positions: Mo1 at  $(1/3, 2/3, z)$ , Mo2 at  $(0, 0, z)$ , and N  $(1/3, 2/3, z)$ . We used the Debye scattering equation<sup>22</sup> to calculate the PDF of single slab using the DiffPy-CMI program.<sup>19</sup> The intralayer structure was refined to better fit the measured PDF of  $Mo_2N$  over the low- $r$  range (1.5 to 5.5 Å). Starting from the carbide  $Mo_2C$  MXene precursor structure, the  $Mo_2N$  slab is squeezed along in-plane dimensions and extended along the out-of-plane dimension ( $z$ -direction) such that the distance between nearest Mo atoms on the same  $z$ -coordinate plane, for example Mo1-Mo2 in Fig. 2c, decreases from 3.3 Å to 2.9 Å, while the distance between nearest Mo atoms separated along the  $z$ -direction (but still within a single slab, e.g. Mo1-Mo3 in Fig. 2c) increases from 2.7 Å to 3.2 Å. The simulated PDF of the initial  $Mo_2N$  model before structure refinement, which has the same atomic positions as the precursor  $Mo_2C$

model, is shown by the brown curve in Fig. 2d. It shows that ammoniation of  $\text{Mo}_2\text{C}$  changes the structure. The  $\text{Mo}_2\text{N}$  structure has the opposite of the distortion to the one in  $\text{Mo}_2\text{C}$  where the out-of-plane Mo-Mo distances are shorter than the in-plane Mo-Mo distances.

### 7 Transmission Electron Microscopy

Transmission Electron Microscopy (TEM) images were performed on JEOL2100F High Resolution TEM, at an accelerating voltage 200 kV. For TEM specimens, the multilayered MXenes ( $\text{Mo}_2\text{CT}_x$  and  $\text{V}_2\text{CT}_x$ ) (not the delaminated MXenes as with all other measurements in this study) were ammoniated at 600 °C for 1 h. The nitride powders were subsequently stirred in an ethanol solution to form a diluted colloidal solution of nitride flakes. The TEM specimens were then prepared by dropping 3 drops of this colloidal solution onto a copper grid and drying in air.

### 8 Electrical Resistivity Measurements

Electronic properties of  $\text{Mo}_2\text{CT}_x$  and  $\text{V}_2\text{CT}_x$  before and after Ar and  $\text{NH}_3$  heat treatment were studied in a Quantum Design EverCool II Physical Property Measurement System (PPMS). Free-standing films with a thickness of about 20  $\mu\text{m}$  of each sample were cut to a 5 × 5 mm squares, and silver wires were attached onto each film in a 4-point probe geometry using adhesive silver paint. In-plane temperature-dependent resistivity was recorded from room temperature (300 K) down to 10 K in vacuum (~20 Torr) in a helium environment. The resistivity values were calculated according to:

$$\rho = \frac{\pi}{\ln 2} \times R \times t \times FF$$

Where  $\rho$  = resistivity ( $\Omega \text{ cm}$ ),  $R$  = resistance ( $\Omega$ ),  $t$  = film thickness (cm),  $FF$  = a correction factor based on the ratio of the probe distance to the film's dimension.

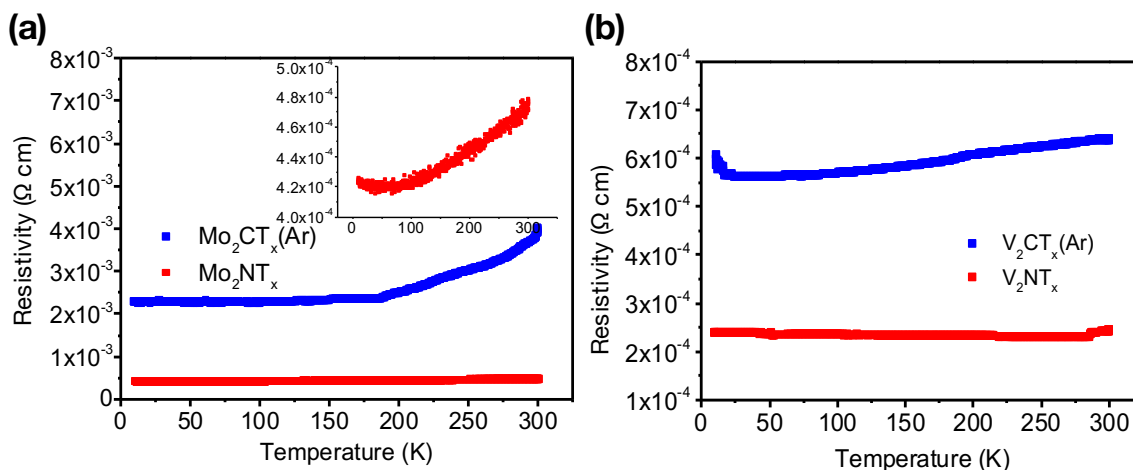


**Figure S8.** A zoom-in portion of the temperature-dependent resistivity of (a)  $\text{Mo}_2\text{CT}_x(\text{Ar})$  and  $\text{Mo}_2\text{NT}_x$  and (b)  $\text{V}_2\text{CT}_x(\text{Ar})$  and  $\text{V}_2\text{NT}_x$ .



## References and Notes

- 1 J. Halim, S. Kota, M. R. Lukatskaya, M. Naguib, M. Q. Zhao, E. J. Moon, J. Pitock, J. Nanda, S. J. May and Y. Gogotsi, *Advanced Functional Materials*, 2016, **26**, 3118-3127.
- 2 M. Naguib, J. Halim, J. Lu, K. M. Cook, L. Hultman, Y. Gogotsi and M. W. Barsoum, *Journal of the American Chemical Society*, 2013, **135**, 15966-15969.
- 3 J. Halim, S. Kota, M. R. Lukatskaya, M. Naguib, M. Q. Zhao, E. J. Moon, J. Pitock, J. Nanda, S. J. May and Y. Gogotsi, *Advanced Functional Materials*, 2016.
- 4 R. Sanjinés, C. Wiemer, J. Almeida and F. Levy, *Thin Solid Films*, 1996, **290**, 334-338.
- 5 J. Halim, K. M. Cook, M. Naguib, P. Eklund, Y. Gogotsi, J. Rosen and M. W. Barsoum, *Applied Surface Science*, 2016, **362**, 406-417.
- 6 M. Romand and M. Roubin, *Analisis*, 1976, **4**, 308-312.
- 7 A. P. Dementjev, A. de Graaf, M. C. M. van de Sanden, K. I. Maslakov, A. V. Naumkin and A. A. Serov, *Diamond and Related Materials*, 2000, **9**, 1904-1907.
- 8 J. Kasperkiewicz, J. Kovacich and D. Lichtman, *Journal of electron spectroscopy and related phenomena*, 1983, **32**, 123-132.
- 9 A. Glaser, S. Surnev, F. Netzer, N. Fateh, G. Fontalvo and C. Mitterer, *Surface Science*, 2007, **601**, 1153-1159.
- 10 A. Pashutski and M. Folman, *Surface Science*, 1989, **216**, 395-408.
- 11 M. Stoica, G. N. B. M. de Macedo and C. Rüssel, *Optical Materials Express*, 2014, **4**, 1574-1585.
- 12 P. J. Chupas, X. Qiu, J. C. Hanson, P. L. Lee, C. P. Grey and S. J. Billinge, *Journal of Applied Crystallography*, 2003, **36**, 1342-1347.
- 13 A. Hammersley, S. Svensson, M. Hanfland, A. Fitch and D. Hausermann, *International Journal of High Pressure Research*, 1996, **14**, 235-248.
- 14 P. Juhás, T. Davis, C. L. Farrow and S. J. Billinge, *Journal of applied Crystallography*, 2013, **46**, 560-566.
- 15 X. Yang, P. Juhas, C. L. Farrow and S. J. Billinge, *arXiv preprint arXiv:1402.3163*, 2014.
- 16 T. Egami and S. J. Billinge, *Underneath the Bragg peaks: structural analysis of complex materials*, Newnes, 2 edn., 2012.
- 17 T. Proffen and S. Billinge, *Journal of Applied Crystallography*, 1999, **32**, 572-575.
- 18 C. Farrow, P. Juhas, J. Liu, D. Bryndin, E. Božin, J. Bloch, T. Proffen and S. Billinge, *Journal of Physics: Condensed Matter*, 2007, **19**, 335219.
- 19 P. Juhás, C. L. Farrow, X. Yang, K. R. Knox and S. J. Billinge, *Acta Crystallographica. A*, 2015, **71**, 562-568.
- 20 A. N. Christensen and B. Lebech, *Acta Crystallographica Section B: Structural Crystallography and Crystal Chemistry*, 1979, **35**, 2677-2678.
- 21 S. Hosoya, T. Yamagishi and M. Tokonami, *Journal of the Physical Society of Japan*, 1968, **24**, 363-367.
- 22 P. Debye, *Annalen der Physik*, 1915, **351**, 809-823.